Agricultural bio-waste of corn silk-derived porous carbon for high-performance supercapacitors

by Rika Taslim

Submission date: 13-Apr-2023 10:45AM (UTC+0700)
Submission ID: 2063153034
File name: 9._Taslim_et_al_2022-Corn_silk.pdf (1.43M)
Word count: 5761
Character count: 29654

IOP Publishing | Vietnam Academy of Science and Technology Advances in Natural Sciences: Nanoscience and Nanotechnology

Adv. Nat. Sci.: Nanosci. Nanotechnol. 13 (2022) 045004 (9pp) https://doi.org/10.1088/2043-6262/ac9c52

Agricultural bio-waste of corn silk-derived porous carbon for high-performance supercapacitors

Rika Taslim[1,*], Suryandri Halbi[1], Apriwandi Apriwandi[2] and Erman Taer[2]

[1] Department of Industrial Engineering, State Islamic University of Sultan Syarif Kasim, 28293 Simpang Baru, Riau, Indonesia

[2] Department of Physics, Faculty of Mathematics and Natural Sciences, University of Riau, 28293 Simpang Baru, Riau, Indonesia

E-mail: rikataslim@gmail.com

Received 19 June 2022
Accepted for publication 11 September 2022
Published 31 October 2022

Abstract

This study aims to develop a novel, simple, efficient, and low-cost method to prepare hierarchical porous carbon nanofiber derived from corn silks (CSAC) through a one-step carbonisation-physical activation process. The carbon precursors were activated by KOH solution at a high pyrolysis temperature to prepare activated porous carbon as an electrode material for supercapacitors without using binders. This study focused on the effect of different activation temperatures of 600, 700, 800, and 900 °C on the production of highly porous carbon nanofiber. An enhancement mechanism is proposed, which not only performed high nanofiber structures to possess the large specific active surface area to enhance energy density but also achieved micro-mesopore combination to realise fast ion-transport channels for boosting high power density. A maximum specific surface area of approximately 1096.95 $m^2 g^{-1}$ was achieved by CSAC7. Furthermore, the electrochemical performance was evaluated using 1 M H_2SO_4 solution as an electrolyte through a novel two-electrode binder-free system. The electrode materials produced a maximum specific capacitance of 237 $F g^{-1}$ at a current density of 1 $A g^{-1}$. These excellent characteristics show that the synthetic approach has a great potential for fabricating high-performance supercapacitors.

Keywords: nanofiber, porous carbon, electrode material, supercapacitor
Classification numbers: 5.16, 5.18

1. Introduction

Supercapacitors are globally considered as superior storage devices due to the higher energy and power density compared to batteries, capacitors, and fuel cells [1]. In addition, they function as suitable materials for electrical components, pulse laser systems, and other electronic devices [2]. Supercapacitors are also directly utilised or combined with batteries for certain electrical facilities, such as electric braking, starters, vehicle, and generators [3]. The electric double-layer capacitors (EDLC) are considered to be the best type due to the variable and adaptable active materials, low cost, abundant availability, superior material properties, maximum electrolyte flow rate, high operating temperature and conductivity, compatibility with a variety of low and high current components, environmental friendliness, and relative safeness [4]. However, supercapacitors still have various challenges such as the relatively low energy compared to the high power density, expensive active materials, and complex synthetic methods. In different studies, the energy density of supercapacitors has been increased with various approaches, but with a reduced power density. The main key to improve the performance of supercapacitors is the active electrode material, followed by the electrolyte and separator [5]. Three groups of active electrode materials have been reported including conduction polymers, metal oxides, and carbon [6].

* Author to whom any correspondence should be addressed.

Conducting polymer materials and metal oxides were used to successfully increase the energy density up to 200 Wh kg^{-1} [7] which is several times greater than the result from other studies in the last decade. However, both materials require complex, complicated, corrosive, and toxic instruments, hence, they are not recommended for environmentally friendly mass production. Therefore, activated carbon from biomass and bio-organic waste is more promising as it has superior and attractive characteristics including abundant availability, renewability, easy fabrication, and low cost [8, 9]. Activated carbon materials also have a good performance in increasing and maintaining energy density, although the energy density produced is still relatively low compared to metal oxides and conduction polymers [10]. Additionally, biomass precursors rich in structurally diverse porosity and significant heteroatoms provide a large number of active ion contacts and facilitate the transport of electrolytic ion charges in various pores including micro-, meso-, and macropores leading to a high performance of energy and balanced power density [11].

Moreover, the 3D hierarchical pore structure obtained from the biomass-derived activated carbon has been shown to increase the energy density up to 5 times coupled with a high power density [12]. Hierarchical porous carbon consisting of micro-, meso-, and macropores are obtained from various biomass precursors such as onion peel [13], pineapple leaves [14], rice husk [15], ginger waste [16], peanut shells [17], bamboo stem [18], and jujube fruit [19]. The peanut shell agricultural biomass produced activated carbon having a 3D hierarchical pore structure as well as abundant micropores and mesopores with surface area about 2014.6 $m^2 g^{-1}$. Activated carbon is prepared by a new and low cost method using $ZnCl_2/CO_2$ activation which produced a specific capacitance of 310 F g^{-1} in a 3-electrode system [20]. Shang *et al,* (2021) obtained activated carbon from chitin (*Portunus trituberculatus* Crab) waste [21], which was converted into hierarchical porous carbon through ZIF-8 nanoparticles bio-template followed by high-temperature carbonisation, leading to a specific capacitance of 182 F g^{-1}. Similar results were also obtained from different biomass precursors such as cauliflower which produced a unique hierarchical pore structure using KOH activation at 700 °C high-temperature which possessed a high surface area of 2061 $m^2 g^{-1}$ [22]. However, the activated carbons obtained from the above precursors are prepared in powder form, hence, they require synthetic binders and insulators to test the electrochemical properties. Although the counter electrodes used are good conduction materials, it is still considered to reduce the efficiency. Also, the template/bio-template method often used to ascertain the 3D pore structure is a relatively risky technique because the final step requires more treatment to remove the by-products. On the other hand, corn silk agricultural biomass has high potential as a hierarchical porous carbon precursor. The basic fibrous structure allows the discovery of dense nanofibers on activated carbon, thereby adding to its renewability. Although the use of corn silk as a starting material for activated carbon in supercapacitors has been previously reported, the method of preparation using binders through a relatively complicated technique is considered to limit its novelty. Therefore, this study aims to prepare binder-free activated carbon through a novel one-step activation of KOH/CO_2. The chosen strategy has been shown to produce higher capacitance compared to Mitravinda *et al* (2018) [23] which used different methods and possesses higher energy density compared to a study by Zhou *et al* (2020) [24]. In addition, we selected H_2SO_4 aqueous electrolytes because of their advantages including the highest ionic concentration, highest conductivity, and low viscosity compared to other aqueous electrolytes. In result, the optimum specific capacitance of activated carbon obtained is 237 F g^{-1} with a maximum energy density of 18.19 Wh kg^{-1} in an aqueous electrolyte of 1 M H_2SO_4.

2. Materials and methods

The corn silks (CS) were initially obtained from the traditional plantations of the Kampar community, Riau and then cut into small pieces within a range of 2 cm, cleaned, and Sundried for 48 h to obtain dry samples. Furthermore, the samples were pre-carbonised and crushed using a crusher machine to obtain dried corn silk powder. The KOH activating agent, HCl, and aqueous electrolyte H_2SO_4 were obtained from Merck KGaA, 4271 Darmstadt, Germany, and Panreac Quimica Sau, Espana, while deionised water (DI) as a material for neutralising samples was made on a lab scale. The organic separator from the duck eggshell membrane was extracted with 1 M HCl solution.

30 g of dried corn silk powder was dispersed with a 5 m l KOH solution on a hotplate at 300 rpm for 2 h. The sample was filtered and dried in an oven at 110 °C, while the corn silk powder was converted into pellets using a hydraulic press without using any adhesive, hence, the adhesive properties of the pure powder were derived originally from the sample. A total of 20 pellets samples were prepared for pyrolysis using carbonisation in the N_2 gas environment and physical activation with CO_2 in the furnace tube. In addition, the pyrolysis process began from a temperature of 30 °C to 600 °C in N_2 gas and then increased to 900 °C in a CO_2 environment. Four different carbonisation temperatures were applied namely 600, 700, 800, and 900 °C. Moreover, to facilitate data interpretation, samples were labelled CSAC-*x*, CSAC was corn silk activated carbon (CSAC), while *x* was the number 6, 7, 8, and 9 indicating carbonisation at the four temperatures. The pelleted carbon samples were neutralised using DI water.

The carbon pellets' density was evaluated based on changes in mass, thickness, and diameter during the pyrolysis process through standard equations. Furthermore, the amorphous properties of the samples were characterised using the X-ray diffraction (XRD) technique at $2\theta = 5°–60°$ with a Cu-K_α radiation source (Phillips expert powder instrument). Surface morphology and distribution of sample elements were also examined through the SEM-EDS (scanning electron microscopy-energy dispersive spectroscopy) technique using the JEOL-JSM-LA-3600 instrument at a voltage of 15 kV. Additionally, the specific surface area and pore diversity were

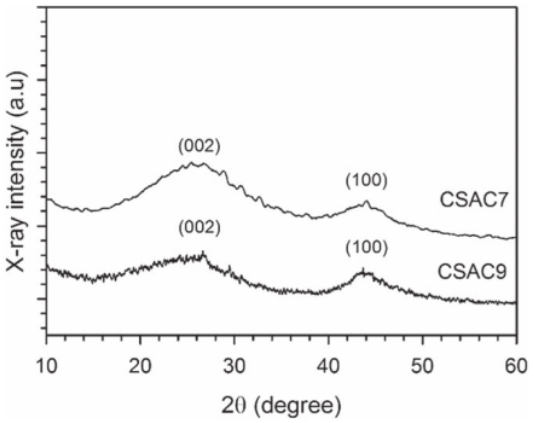

Figure 1. The XRD pattern of CSAC7 and CSAC9.

determined through the N_2 gas absorption technique and evaluated using BET and BJH calculations.

The electrochemical properties of the supercapacitor were evaluated in two-electrode configurations. The supercapacitor cells were made in the form of sandwich layers consisting of a cell body made of acrylic, stainless steel current collector, pelleted carbon electrodes, and an organic separator from the duck eggshell membrane. Interestingly, the semi-permeable duck eggshell membrane allows the electrolyte ions to diffuse ionally on the surface of the carbon electrode [25]. The cyclic voltammetry (CV) and galvanostatic charge-discharge (GCD) methods are techniques commonly used in evaluating specific capacitan as well as energy and power density. CV was evaluate using the CV-UR Rad-Er 1380 instrument at a constant voltage range of 0–1.0 V at a scan rate of 1 mV s^{-1}, while GCD used the 2018 CD-UR Rad-Er at a fixed current of 1 A, both instruments were calibrated with a mean error of ±6.01%.

3. Results and discussions

Crystal phase change properties of corn silk-based hierarchical porous carbon were reviewed using the powder XRD method. The XRD patterns with different physical activation temperatures particularly between 700 and 900 °C are shown in figure 1.

The CSAC7 display two clearly confirmed broad peaks at $2\theta = 24.34$ and 43.92° which correspond to the (002) and (100) scattering planes. These characteristics show that the structure of the turbostratic/disturbed carbon has a high amorphous nature [26]. This property is important for improving the good hierarchical pore structures in carbon samples. On the other hand, CSAC9 performed low broad peaks at $2\theta = 24.86$ and 44.13° indicating the amorphous nature degraded towards graphitisation due to high-temperature treatment. Furthermore, the most obvious broad peaks in the (002) reflection plane ranging between angle 24.34°–24.86° indicate a random aromatic sheet structure, while the (100) reflection plane from 43.92 to 44.13° confirms the type of carbon that is close to the graphite structure, in this case, the attenuation of the graphite structure towards the formation of a disturbed carbon structure [27].

The morphological structure of activated carbon-based corn silk waste was evaluated using the SEM method at a voltage of 15 kV. Figure 2 shows the morphological structure with different physical activation temperatures of 600, 700, 800, and 900 °C. In general, the surface structure of the sample is dominated by bulk materials, aggregation and clumps of large wrinkled particles, while some parts display a different inner surface structure for each temperature. At 600 °C (figure 2(a)), the activated carbon consisted of particle aggregations with surface wrinkles. Additionally, a larger zoom in figure 2(b) shows that the sample surface is relatively flat in each aggregation without any obvious pores. Furthermore, comparatively to 600 °C, physical activation at a higher temperature led to a better decomposition into the basic components such as hemicellulose, cellulose, and lignin. This ficates a relatively different surface morphology as shown in figures 2(c) and (d). Figure 2(c) shows the relatively dominant pore hole structure in the 64–7214 nm range. The diverse pore structures including mesopores and macropores were confirmed at a larger magnification area as shown in figure 2(d). Mesopores have a size ranging from 18–48 nm, while macropores are in the range of 73–136 nm. Howe micropore structures were not found at this magnification. An increase in the physical activation temperature of 800 °C in the CSAC8 sample shows a surface morphology filled with macropores whic ave a relatively large size less than 300 nm as shown in figure 2(e). In addition, figure 2(f) shows a distinct morphology in which clustered tubular-rod-like structures are found. This is because the higher temperature porosity allows the breakdown of the main carbon structure derived from cellulose and lignin drastically. The rod shape is contributed from the basic structure of cellulose while the outer tubular shape is attributed to lignin [28]. This analysis has been reported in previous studies with different biomass precursors such as cassava petiole [29] and cacao shells [30]. Moreover, the temperature of 900 °C maximised the basic decomposition process of cellulose and lignin to form a clear surface morphology of carbon fibers, as shown in figures 2(g) and (h). The diameter of the obtained nanofibers varied relatively in the range of 76–127 nm. The predominant nanofiber fiber allows well-connected pores in a relatively small size range [31]. The emental composition of porous activated carbon samples at activation temperatures of 700 and 900 °C for CSAC7 and CSAC9 was examined using energy dispersive spectrosco (EDS) techniques in the energy range of 0–20 keV. Table 1 shows the elemental composition of the CSAC7 and CSAC9 samples in detail. Elemental carbon (C) has the highest percentage of approximately 83.75%–85.28% followed by oxygen 8.03%–8.61%, silicon (Si) 3.15%–3.25%, potassium (K) 1.64%–3.94%, magnesium (Mg) 0.79%–0.83%, and aluminium (Al) 0.33%–0.40%.

High-temperature pyrolysis of 700 °C for CSAC7 showed the highest carbon composition of 85.28%. This

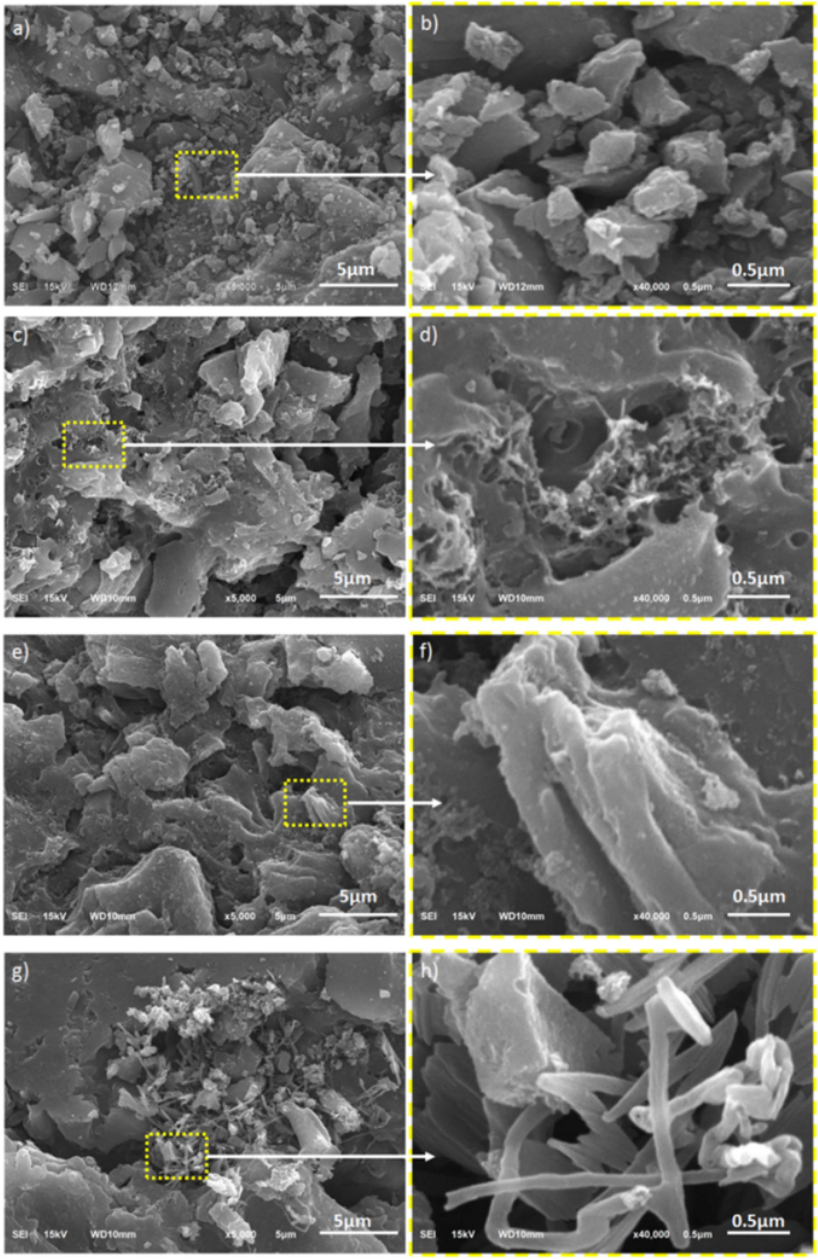

Figure 2. The SEM images of CSAC6 in magnification of (a) 5000*x*, (b) 40000*x*, CSAC7 in magnification of (c) 5000*x*, (d) 40000*x*, CSAC8 in magnification of (e) 5000*x*, (f) 40000*x*, CSAC9 in magnification of (g) 5000*x*, (h) 40000*x*.

Table 1. The elemental composition of CSAC7 and CSAC9.

Element	C (%)	O (%)	Si (%)	K (%)	Mg (%)	Al (%)
CSCA7	85.28	8.61	3.25	1.64	0.83	0.40
CSAC9	83.75	8.03	3.15	3.94	0.79	0.33

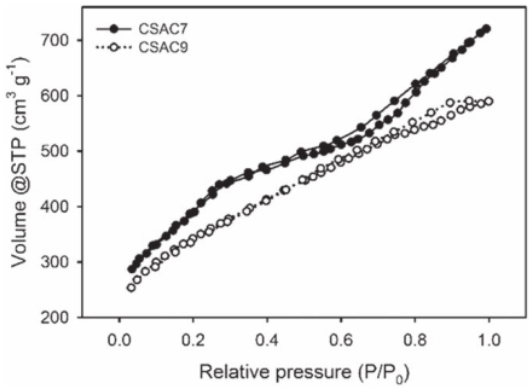

Figure 3. Nitrogen adsorption-desorption isotherms of CSAC7 and CSAC9.

property is considered to increase the capacitive properties of the electrode material. Furthermore, the highest elemental oxygen was also found in the CSAC7 sample which contributed to the wettability of the material, thereby initiating the pseudocapacitance effect [32]. An increase in the activation temperature up to 900 °C for CSAC9 reduced the percentage of carbon and oxygen in the sample. This is because the activation of high temperatures evaporates the constituent elements of the material in the form of more H_2O and CO_2. Moreover, other elements such as Si, K, Mg, and Al are obtained in relatively low amounts from basic sources of biomass that have not been completely evaporated [33].

The analysis of N_2 adsorption/desorption isotherms of corn silk-based hierarchical porous activated carbon at different pyrolysis temperatures is needed to evaluate the impact of pore structure and porosity properties. Figure 3 shows the N_2 adsorption-desorption isotherm curve of both samples, CSAC7 had significant N_2 adsorption at a relative pressure of $0 < P/P_0 < 0.2$, thereby confirming the relatively large number of micropores.

Furthermore, the H4 type hysteresis loop was clearly shown over a relatively long relative pressure range of $0.2 < P/P_0 < 0.9$ indicating uniform mesoporous characteristics at CSAC7 as presented in table 2. The tail at high-pressure $P/P_0 > 0.9$ shows the presence of macropores, but the addition of the physical activation temperature up to 900 °C in CSAC9 showed a different N_2 isotherm absorption compared to CSAC7. The N_2 adsorption-desorption curve of CSAC9 shows a relatively linearly increasing adsorption which is not too high at low pressure, thereby indicating the presence of low micropores. In addition, the H4 type hysteresis loop is not formed completely at a relatively short pressure range of P/P_0 about 0.6–0.95 which is mainly due to the pores growing towards the larger one and is dominated by narrow bottle neck-like types with a larger inner surface [34] as shown in table 2. The pore size distribution as presented in figure 4 shows that both samples have a combination of micropores and macropores. This result is relatively consistent with SEM which also confirms the hierarchical porous structure. CSAC7 has a structure of hierarchically connected 3D pores leading to the presence of mesopores with a peak at 3.89 nm. Furthermore, the chemical impregnation of KOH at 700 °C high-temperature pyrolysis allows the precursor to produce a good combination of micropores and mesopores to improve the performance of the base electrode.

The microporous and mesoporous percentages of CSAC7 are 48.41 and 51.59% with a high surface area of 1096.95 $m^2\ g^{-1}$. The high surface area coupled with the combination of the hierarchically connected pores is believed to improve the electrochemical properties of supercapacitors [35]. In addition, the high mesoporous volume fraction potentially facilitates rapid ion transport and acts as an electrolyte ion reservoir, thereby reducing the ion diffusion distance to the carbon surface, ensuring high rate capability and high power density. Moreover, CSAC9 displays a relatively similar pore size distribution with CSAC7 but is dominated by micropores with a percentage of 56.84%. KOH impregnation at higher temperatures up to 900 °C allows degradation of carbon aggregation and erodes the main pore walls, thereby creating tubular and nanofiber structures. This simultaneously reduces the specific surface area of CSAC9 to 744.82 $m^2\ g^{-1}$ with an average diameter of 3.2 nm as shown in table 2. Nevertheless, the developed porosity properties of carbon materials are important for electrolyte ions' rapid transport and penetration [36]. These results are consistent with the SEM and density data.

The main parameters used to evaluate the electrochemical properties of hierarchical porous activated carbon include high specific capacitance, increased energy and fixed power density, as well as retention capacitance. Based on the N_2 gas absorption analysis, the corn silk-based activated carbon has a combination of micropores and mesopores that is able to accommodate a relatively high charge of active ions and facilitate diffusion without obstruction at the electrode/electrolyte interface. The electrochemical performance of CSAC6, CSAC7, CSAC8, and CSAC9 based on different physical activation temperatures was evaluated with a two-electrode configuration in an aqueous electrolyte using cyclic voltammetry and galvanostatic charge-discharge techniques. CV curves at 600, 700, 800, and 900 °C are shown in figure 5. The CV profile exhibits a quasi-rectangular shape, indicating the typical behaviour of electrochemical double-layer supercapacitors (EDLC) in an aqueous electrolytic system at a scan rate of 1 $mV\ s^{-1}$.

In addition, the pseudocapacitance property was found to be relatively low as indicated by a spike in current density of the voltage ranging from 0.3–0.6V. This property is a contribution of the heteroatom and wettability properties of elemental oxygen in the sample. In general, all samples exhibited similar electrochemical properties. By using standard equations, the specific capacitances of CSAC6, CSAC7, CSAC8, and CSAC9 were evaluated to be 184, 211, 194, and 143 $F\ g^{-1}$, respectively. An increase in the physical activation temperature improved the capacitive properties of the supercapacitor by 211 $F\ g^{-1}$. This is because the higher temperature of CSAC7 showed a relatively rich surface structure of mesopores and macropores, which provides a high surface

Table 2. Specific surface area, pore volume and average pores size of CSAC7 and CSAC9.

Sample	S_{BET} ($m^2\,g^{-1}$)	S_{micro} ($m^2\,g^{-1}$)	S_{meso} ($m^2\,g^{-1}$)	V_{tot} (cm^3/g)	V_{micro} ($cm^3\,g^{-1}$)	V_{meso} ($cm^3\,g^{-1}$)	D_{aver} (nm)
CSAC7	1096.95	531.09	565.86	1.12	0.31	0.80	4.1
CSAC9	744.82	423.36	321.46	0.91	0.45	0.46	3.2

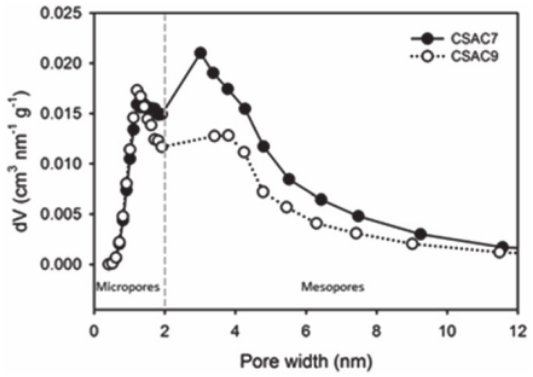

Figure 4. Pore sizes profile of CSAC7 and CSAC9.

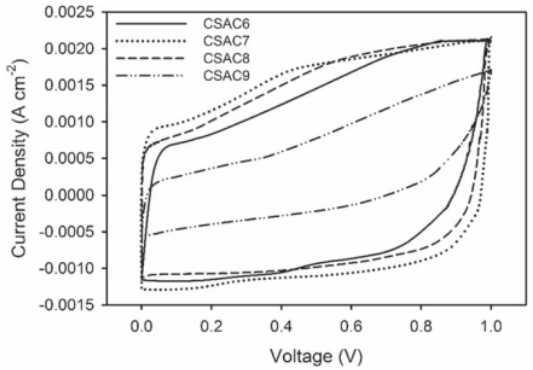

Figure 5. CV curves of CSAC6, CSAC7, CSAC8, and CSAC9.

area and diffusion path of ionic charge in all directions, thereby facilitating the high capacitive properties. This analysis is consistent with SEM results and N_2 gas absorption in figures 2 and 3. At 800 °C, the surface structure of the capacitive properties was reduced to 194 F g^{-1}. This is because the increase in the physical activation temperature in the CSAC8 sample shows a surface morphology filled with macropores with a relatively large size less than 300 nm, as shown in figure 2(e). In addition, the morphology of the clustered tubular rod-like structure allows the fractures that narrow the ion transport pathways on the electrode surface.

A further temperature increase up to 900 °C for CSAC9 allows the erosion and breakdown of the particle walls of carbon aggregation and rod-like structures to cover the existing pores, this reduced the capacitive properties to 143 F g^{-1}. Although the pore structure displays relatively dense nanofibers as shown in figure 2(h), it is unable to maintain the

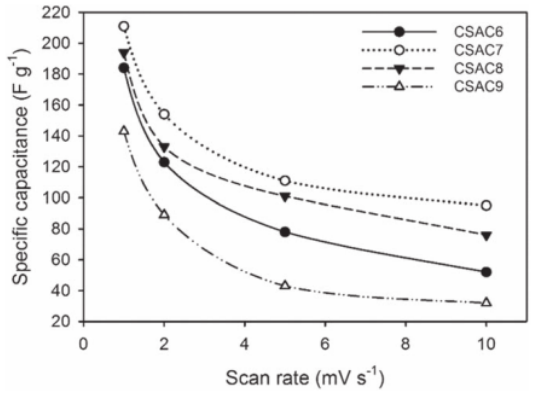

Figure 6. The curves of specific capacitance vs. scan rate of CSAC6, CSAC7, CSAC8, and CSAC9.

3D hierarchical pore distribution of micropores and mesopores, thereby reducing the electrochemical properties. The specific capacitances of CSAC6, CSAC7, CSAC8, and CSAC9 were also evaluated at different scan rates from 1 to 10 mV s^{-1}, as shown in figure 6. The activated carbon which maintained the highest specific capacitance of 45% was CSAC7, followed by CSAC8, CSAC6, and CSAC9 with values of 39, 28, and 23%, respectively. The galvanostatic charge-discharge (GCD) curves of symmetric cells CSAC6, CSAC7, CSAC8, and CSAC9 at a current density of 1 A g^{-1} are shown in figure 7(a). In general, the GCD curve displays a normal profile for the EDLC type with a slightly faint IR drop. According to the GCD profile, the specific capacitances produced at CSAC6, CSAC7, CSAC8, and CSAC9 were 152, 237, 174 and 124 F g^{-1}, respectively, in the electrolyte of 1 M H_2SO_4. Higher activation temperature from 600 to 700 °C confirmed that micro-mesopore combinations of 48.41 and 51.59% displayed the highest electrochemical properties from 152 to 237 F g^{-1}. These results correlate with SEM, N_2 gas adsorption/desorption, and CV analysis. The high activation temperature of from 700 to 900 °C decreased the capacitive value of the carbon electrode up to 124 F g^{-1} for the CSAC9 sample. This is associated with the collapse of the pore walls and the erosion of the carbon framework structure to cover the active site of the ionic charge below [34].

Furthermore, the resistance in CSAC7 was lower at 0.0025 Ω due to the relatively high dominance of the mesopores which improved the diffusion of ionic charges in all directions compared to CSAC6, CSAC8, and CSAC9 which have a higher resistance value of 0.012, 0.27, and 0.034 Ω, respectively. This is also contributed by the semi-permeable duck eggshell membrane which allows the electrolyte ions to

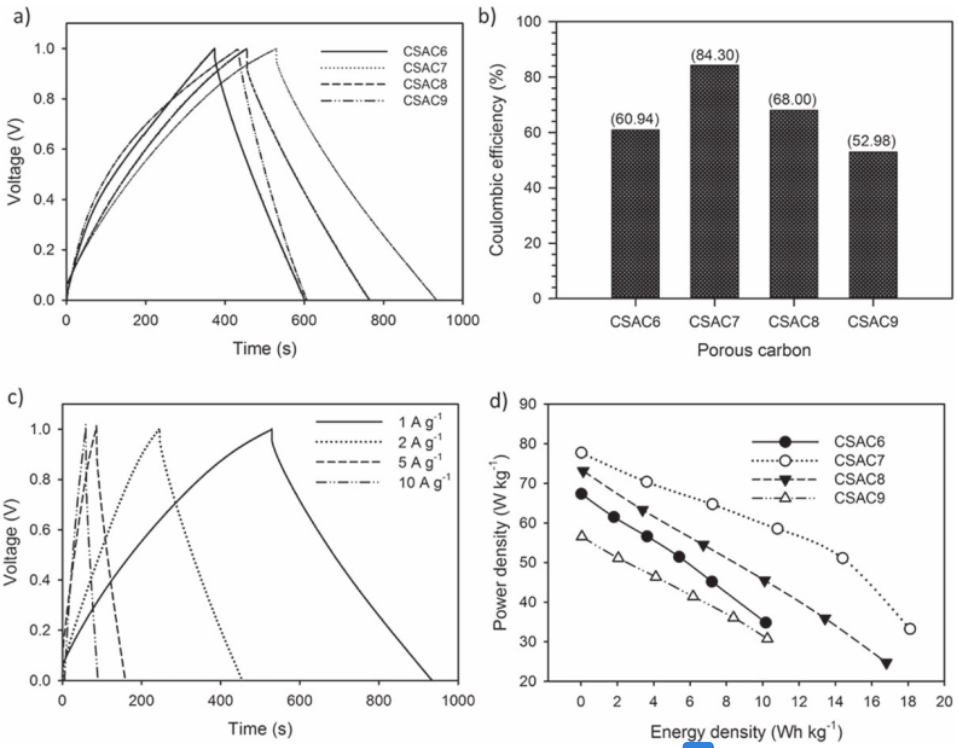

Figure 7. (a) GCD curves, (b) Coulombic efficiency of CSAC6, CSAC7, CSAC8, and CSAC9, (c) GCD curves at different current densities of CSAC7, and (d) Ragone plot of CSAC6, CSAC7, CSAC8, and CSAC9 in 1 M H_2SO_4 electrolyte.

diffuse optimally on the surface of the carbon electrode [25]. In addition, the charge and discharge times on the GCD profiles reflect the coulombic efficiency of GLACs, as shown in figure 7(b). CSAC7 had the highest coulombic efficiency of about 84.30%, followed by CSAC8, CSAC6 and CSAC9 of 68.00, 60.94, and 52.98%, respectively which confirmed the high collective interpenetration and accessibility of the electrolyte. Moreover, the GCD profile of CSAC7 was reviewed at different current densities of 1, 2, 5, and 10 A g^{-1}, as shown in figure 7(c). It can be noted that the GCD curves of CSAC7 still maintain primary symmetric triangle shape at 10 A g^{-1}, suggesting stable double-layer capacitor behaviours, fast response, and low internal resistance in EDL processes. At 1 A g^{-1}, CSAC7 sample delivers a specific capacitance of 237 F g^{-1} and it still maintains 210 F g^{-1} at 10 A g^{-1}, initiating a high-rate performance of 88.6%.

To compare the performance of both samples in depth, Ragone plots were used to evaluate the energy and power density which are calculated using standard formulas as shown in figure 7(c). Symmetrical supercapacitors CSAC6, CSAC7, CSAC8, and CSAC9 assembled with an aqueous electrolyte of 1M H_2SO_4 in an organic separator had energy densities of 10.17, 18.11, 16.81 and 10.26 Wh kg^{-1} as well as power densities of 67.38, 77.74, 73.14 and 56.54 W kg^{-1}, respectively. The high electrochemical capability of CSAC7 is due to the 3D hierarchical porous structure and the specific surface area which provides a short and accessible ion transfer area in all directions for ionic charges to diffuse at the electrode/electrolyte interface.

The high electrochemical confirmation of CSAC7 was reviewed in depth via a Nyquist plot with a limited diffusion area in the frequency range of 0.01 Hz to 100 kHz, as shown in figure 8(a). Horizontal translation along the Z' axis confirms a relatively low Rs of 0.87 Ωcm^2, indicating a good ions adsorption and desorption process at the electrode-electrolyte interface. Furthermore, the RCT (12.3 Ωcm^2) interpreted at the semicircular position confirmed the fast charge transfer kinetically as a result of the current passing through the electrode forming an electric layer. This is because the hierarchical pore structure with a combination of micro-, meso-, and macropores initiates the active site which is followed by the ability of ion diffusion in all directions without any obstacles. In addition, the straight line that tends to be perpendicular at low frequencies confirms the pure capacitive and high ion transfer rate at the CSAC7 electrode. The Bode phase angle plot of CSAC7 was also evaluated as shown in figure 8(b). The phase angle at low frequencies reveals specific information about the ability of the electrode to generate an electric double layer. CSAC7 electrode displays a phase angle close to −90°, indicating that the normal dielectric layer

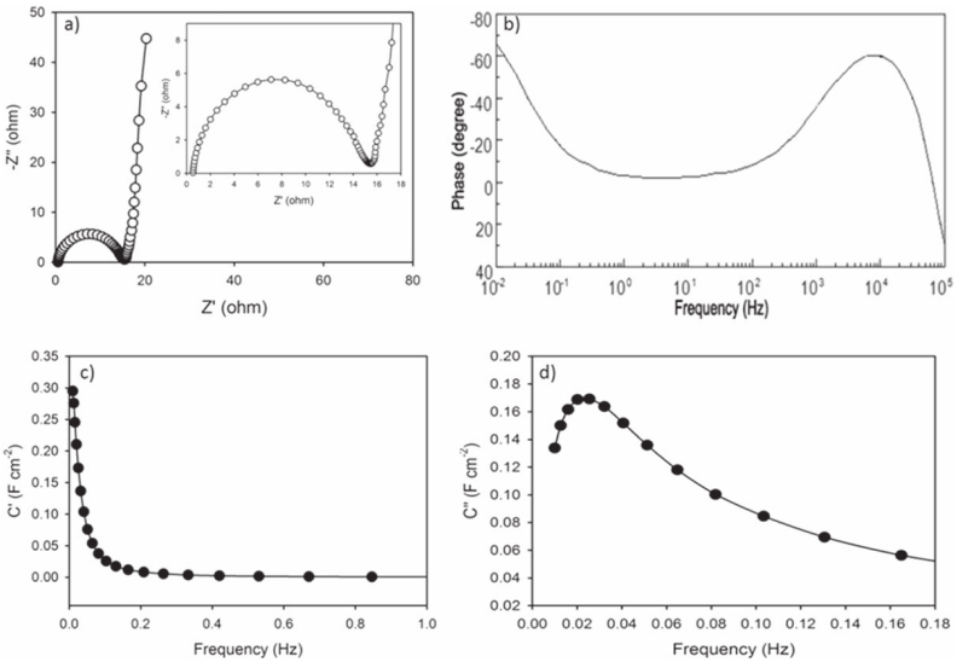

Figure 8. (a) Nyquist plot, (b) Bode phase angle plot, (c) real capacitance (C') versus frequency plot, and (d) imaginer capacitance (C'') vs. frequency plot of CSAC7 symmetrical devices.

of the EDLC version is accompanied by impaired ion degradation due to self-heteroatom doping. In addition, the Bode phase angle plot provides further information on the characteristics of the conductive material through analysis of the real capacitance (C'') and the imaginary capacitance (C'') with respect to frequency, as shown in figures 8(b), and (c). The C'' values are weak in the lower frequency and higher frequency regions, the C'' values show less frequency dependence, indicating a purely resistive behaviour in CSAC7. Moreover, the value of the imaginary capacitance C'' at the peak frequency confirms a relaxation time of 9.25 seconds, indicating that the symmetrical CSAC7 device acts as a pure capacitor. This value indicates a measure of how quickly the stored energy of the device can be efficiently distributed. For comparison, the obtained carbon nanofiber based on corn silk waste showed higher electrochemical properties than the carbon nanofiber based on bacterial cellulose and tofu dregs obtained through chemical activation of KOH and H_3PO_4 [37, 38]. In addition, although polymer-based carbon nanofibers exhibit superior specific capacitance, our study was able to produce higher energy densities than the previously reported one as confirmed in reference [39]. This is due to the combination of nanofiber and micro-mesoporous structures allowing the provision of high active sites and ion-transport channels. Moreover, the binder-free electrode design supports the high electrochemical performance of the supercapacitor.

4. Conclusion

Based on the results, hierarchically porous carbon nanofiber was successfully obtained from corn silk using a low-cost, simple, and sustainable technique without a binding material for a high energy density of symmetric supercapacitors. In addition, different physical activation temperatures display distinctive pore structure with individual advantages. At 700 °C, a 3D hierarchical pore structure was displayed, followed by a high surface area leading to the formation of an ideal combination of micro- and mesopores for enhancing the high performance of the electrode material. Using a two-electrode binder-free system, CSAC7 showed the best electrochemical properties with a specific capacitance of 237 F g^{-1} in 1 M H_2SO_4 aqueous electrolyte. Hence, the maximum energy density of 18.19 Wh kg^{-1} and power density of 77.74 W kg^{-1} at current density of 1 A g^{-1} were achieved. This result shows that the approach applied in this study confirmed the potential of corn silk as an activated carbon-based material with high properties.

Acknowledgments

This study was funded by collaborative grants between universities, State Islamic University of Sultan Syarif Kasim Riau with contract No. 873/Un.04/L. 1/TL.01/03/2022.

References

[1] Poonam, Sharma K, Arora A and Tripathi S K 2019 *J. Energy Storage* **21** 801

[2] Kumar R, Sahoo S, Joanni E, Singh R K, Tan W K, Kar K K and Matsuda A 2019 *Prog. Energy Combust. Sci.* **75** 100786

[3] Farma R, Anugrah A P, Apriyani I and Awitdrus A 2022 *Adv. Nat. Sci.: Nanosci. Nanotechnol.* **13** 015009

[4] Hoa L T M 2021 *Adv. Nat. Sci.: Nanosci. Nanotechnol.* **12** 025014

[5] Chaudhary S, Raja M and Sinha O P 2021 *Adv. Nat. Sci.: Nanosci. Nanotechnol.* **12** 015011

[6] Zheng S, Li Q, Xue H, Pang H and Xu Q 2020 *Natl Sci. Rev.* **17** 305

[7] Tiwari S K, Sahoo S, Wang N and Huczko A 2020 *J. Sci. Adv. Mater. Devices* **5** 10

[8] Taer E and Taslim R 2018 *AIP Conf. Proc.* **1927** 020004

[9] Bhat V S, Kanagavalli P, Sriram G, John N S B R, Veerapandian M, Kurkuri M and Hegde G 2020 *J. Energy Storage* **32** 101829

[10] Jay P *et al* 2020 *ECS Meet. Abstr.* **MA2020-01** 1893

[11] Ng D, Nai J, Li H, Xu L and Wang Y 2019 *Carbon* **141** 40

[12] Wang D, Pan Z, Chen G and Lu Z 2021 *Electrochim. Acta* **379** 138170

[13] Mehare M D, Deshmukh A D and Dhoble S J 2020 *J. Mater. Sci.* **55** 4213

[14] Sodtipinta J, Ieosakulrat C, Poonyayant N, Kidkhunthod P, Chanlek N, Amornsakchai T and Pakawatpanurut P 2017 *Ind. Crops Prod.* **104** 13

[15] Chen Z, Wang X, Xue B, Li W, Ding Z, Yang X, Qiu J and Wang Z 2020 *Carbon N. Y.* **161** 432

[16] Liangshuo L, Lin Q, Xinyu L, Ming D and Xin F 2020 *Optoelectron. Adv. Mater. Rapid Commun.* **14** 548

[17] Li X, Li R, Han J, Yu M and Wu M 2013 *Mater. Lett.* **94** 158

[18] Taer E, Pratiwi L, Apriwandi, Mustika W S, Taslim R and Agustino 2020 *Commun. Sci. Technol.* **5** 22

[19] Yang V, Senthil R A, Pan J, Kumar T R, Sun Y and Liu X 2020 *J. Colloid Interface Sci.* **579** 347

[20] Jiang X, Guo F, Jia X, Zhan Y, Zhou H and Qian L 2020 *J. Energy Storage* **30** 101451

[21] Shang Z, An X, Liu L, Yang J, Zhang W, Dai H, Cao H, Xu Q, Liu H and Ni Y 2021 *Carbohydr. Polym.* **251** 117107

[22] Men B, Guo P, Sun Y, Tang Y, Chen Y, Pan J and Wan P 2019 *J. Mater. Sci.* **54** 2446

[23] Mitravinda T, Nanaji K, Anandan S, Jyothirmayi A, Chakravadhanula V S K, Sharma C S and Rao T N 2018 *J. Electrochem. Soc.* **165** A3369

[24] Zhou J, Yuan S, Lu C, Yang M and Song Y 2020 *J. Electroanal. Chem.* **878** 114704

[25] Li W, Chen C, Wang H, Li P, Jiang X, Yang J and Liu J 2022 *J. Mater. Res. Technol.* **17** 1540

[26] Ni W and Shi L 2019 *J. Vacuum Science & Technology A* **37** 040803

[27] Serafin J, Baca M, Biegun M, Mijowska E, Kaleńczuk R J, Sreńscek-Nazzal J and Michalkiewicz B 2019 *Appl. Surf. Sci.* **497** 143722

[28] Ning W, Pan J and Liu X 2019 *J. Power Sources* **409** 13

[29] Taer E, Apriwandi, Dalimunthe B K L and Taslim R 2021 *J. Chem. Technol. Biotechnol.* **96** 662

[30] Taer E, Apriwandi A, Agutino A, Taslim R, Mustika W S and Exa Fadli 2021 *Nanosci. Technol. An Int. J.* **12** 45

[31] Ni W, Shi L and Resol 2022 *Materials Research Foundations* **122** 154

[32] Liu F, Wang Z, Zhang H, Jin L, Chu X, Gu B, Huang H and Yang W 2019 *Carbon N. Y.* **149** 105

[33] Zhou D-D, Zhang X-W, Mo Z-W, Xu Y-Z, Tian X-Y, Li Y, Chen X-M and Zhang J-P 2019 *EnergyChem* **1** 100016

[34] Bai Y, Liu C, Chen T, Li W, Zheng S, Pi Y, Luo Y and Pang H 2021 *Angew. Chem. Int. Ed.* **60** 25318

[35] Surya K and Michael M S 2020 *J. Electroanal. Chem.* **878** 114674

[36] Wang Y, Qiao M and Mamat X 2021 *Appl. Surf. Sci.* **540** 148352

[37] Hao X, Wang J, Ding B, Wang Y, Chang Z, Dou H and Zhang X 2017 *J. Power Sources* **352** 34

[38] Taer E, Hasanah F and Taslim R 2021 *Commun. Sci. Technol.* **6** 41

[39] Li J, Zou Y, Xiang C, Xu F, Sun L, Li B and Zhang J 2021 *J. Energy Storage* **42** 103017

Agricultural bio-waste of corn silk-derived porous carbon for high-performance supercapacitors

ORIGINALITY REPORT

14%	10%	11%	4%
SIMILARITY INDEX	INTERNET SOURCES	PUBLICATIONS	STUDENT PAPERS

PRIMARY SOURCES

1	Rakhmawati Farma, Hafizatul Husni, Irma Apriyani, Awitdrus Awitdrus, Erman Taer. "Biomass Waste-Derived Rubber Seed Shell Functionalized Porous Carbon As an Inexpensive and Sustainable Energy Material for Supercapacitors", Journal of Electronic Materials, 2021 Publication	1%
2	nanoscalereslett.springeropen.com Internet Source	<1%
3	repo.lib.tut.ac.jp Internet Source	<1%
4	www.researchgate.net Internet Source	<1%
5	Yi Zhou, Jun Ma, Jianhong Yang, Zhicheng Lv, Zhiyong Song, Heyou Han. "Soybean rhizosphere microorganisms alleviate Mo nanomaterials induced stress by improving soil microbial community structure", Chemosphere, 2022	<1%

Publication

6	Yuyang Cao, Shiqiang Wei, Quan Zhou, Pengjun Zhang et al. "Ti-Cl Bonds decorated Ti2NTx MXene towards high-performance lithium-ion batteries", 2D Materials, 2022 Publication	<1 %
7	Submitted to Indian Institute of Technology, Madras Student Paper	<1 %
8	R Taslim, A Agustino, E Taer. "Naturalcarbon-metal composite for supercapacitor application", Journal of Physics: Conference Series, 2018 Publication	<1 %
9	Shuli Jiang, Ruiming Huang, Wenchang Zhu, Xiangyi Li, Yue Zhao, Zhixiang Gao, Lijun Gao, Jianqing Zhao. "Free-Standing SnO2@rGO Anode via the Anti-solvent-assisted Precipitation for Superior Lithium Storage Performance", Frontiers in Chemistry, 2019 Publication	<1 %
10	Yinghua Wei, Xiaojuan Chen, Gexiang Gao, Daozheng Shen, Hongren Rong, Qi Liu. "Achieving high-performance aqueous Zn-ion hybrid supercapacitors by utilizing zinc-based MOF-derived N-doped carbon", Ionics, 2022 Publication	<1 %

pubs.rsc.org

11	Internet Source	<1%
12	www.researchsquare.com Internet Source	<1%
13	cst.kipmi.or.id Internet Source	<1%
14	ouci.dntb.gov.ua Internet Source	<1%
15	Akhil Pradiprao Khedulkar, Bidhan Pandit, Van Dien Dang, Ruey-an Doong. "Agricultural waste to real worth biochar as a sustainable material for supercapacitor", Science of The Total Environment, 2023 Publication	<1%
16	Submitted to King Mongkut's Institute of Technology Ladkrabang Student Paper	<1%
17	Aslam Hossain, R. Manu, S.M.A. Shibli. "Chemically Modified Carbon Nanotubes for Tribology Applications", Wiley, 2023 Publication	<1%
18	E Taer, R Radiawan, R Taslim, Awitdrus, A Apriwandi, Krisman, Minarni, A Agustino, R Farma, R N Setiadi. "The effect of microwave irradiation in activated carbon processing from sago waste to physical and	<1%

electrochemical properties of electrode supercapacitor cells", Journal of Physics: Conference Series, 2018
Publication

19	aaqr.org Internet Source	<1 %
20	hal.science Internet Source	<1 %
21	chalcogen.ro Internet Source	<1 %
22	Vinay S. Bhat, Syam G. Krishnan, Titilope John Jayeoye, Thitima Rujiralai et al. "Self-activated ‘green’ carbon nanoparticles for symmetric solid-state supercapacitors", Journal of Materials Science, 2021 Publication	<1 %
23	asmedigitalcollection.asme.org Internet Source	<1 %
24	www.science.gov Internet Source	<1 %
25	snf.fmipa.unri.ac.id Internet Source	<1 %
26	Submitted to Universitas Riau Student Paper	<1 %
27	Xiaojun Ma, Chenfeng Ding, Dongna Li, Mingyue Wu, Yunhua Yu. "A facile approach to	<1 %

prepare biomass-derived activated carbon hollow fibers from wood waste as high-performance supercapacitor electrodes", Cellulose, 2018
Publication

---

28 Yang, J.. "Carbon Electrode Material with High Densities of Energy and Power", Acta Physico-Chimica Sinica, 200801 <1%
Publication

---

29 Zhongkai Wu, Haifu Huang, Wenhui Xiong, Shiming Yang et al. "One-Pot Synthesis of Glucose-Derived Carbon Coated Ni3S2 Nanowires as a Battery-Type Electrode for High Performance Supercapacitors", Nanomaterials, 2021 <1%
Publication

---

30 Shuang Liu, Shubin Wu, Hao Cheng. "Preparation and characterization of lignin-derived nitrogen-doped hierarchical porous carbon for excellent toluene adsorption performance", Industrial Crops and Products, 2023 <1%
Publication

---

31 Submitted to Visvesvaraya National Institute of Technology <1%
Student Paper

---

32 Wang, Zifeng, Yushan Liu, Chengwei Gao, Hao Jiang, and Jianmin Zhang. "A porous Co(OH)2 <1%

material derived from a MOF template and its superior energy storage performance for supercapacitors", Journal of Materials Chemistry A, 2015.
Publication

33	d.lib.msu.edu Internet Source	<1 %
34	www.mdpi.com Internet Source	<1 %
35	www.rsc.org Internet Source	<1 %
36	Guangxu Fu, Huimin Li, Qiuhong Bai, Cong Li, Yehua Shen, Hiroshi Uyama. "Dual-doping activated carbon with hierarchical pore structure derived from polymeric porous monolith for high performance EDLC", Electrochimica Acta, 2021 Publication	<1 %
37	Lei, Zhibin, Nikolay Christov, Li Li Zhang, and X. S. Zhao. "Mesoporous carbon nanospheres with an excellent electrocapacitive performance", Journal of Materials Chemistry, 2011. Publication	<1 %
38	www.acoustics.asn.au Internet Source	<1 %

Submitted to University of College Cork

39	Student Paper	<1%
40	Boryana Karamanova, Antonia Stoyanova, Maria Shipochka, Svetlana Veleva, Radostina Stoyanova. "Effect of Alkaline – Basic Electrolytes on the Capacitance Performance of Biomass-Derived Carbonaceous Materials", Materials, 2020 Publication	<1%
41	ashpublications.org Internet Source	<1%
42	pubs.acs.org Internet Source	<1%
43	spiral.imperial.ac.uk Internet Source	<1%
44	Dattatray S. Dhawale, Sehwan Kim, Dae-Hwan Park, Jin-Ho Choy, Salem S. Al-deyab, Katsuhiko Ariga, Eunkyoung Kim, Ajayan Vinu. "Hierarchically Ordered Porous CoOOH Thin-Film Electrodes for High-Performance Supercapacitors", ChemElectroChem, 2015 Publication	<1%
45	Mirosław Kwiatkowski, Jarosław Serafin, Andy M. Booth, Beata Michalkiewicz. "Computer Analysis of the Effect of Activation Temperature on the Microporous Structure	<1%

Development of Activated Carbon Derived from Common Polypody", Materials, 2021
Publication

46	Perez-Ramirez, J.. "Evolution of isomorphously substituted iron zeolites during activation: comparison of Fe-beta and Fe-ZSM-5", Journal of Catalysis, 20050610 Publication	<1 %
47	Yuyang Cao, Shiqiang Wei, Quan Zhou, Pengjun Zhang et al. " Ti–Cl bonds decorated Ti NT MXene towards high-performance lithium-ion batteries ", 2D Materials, 2022 Publication	<1 %
48	m.researching.cn Internet Source	<1 %
49	mdpi-res.com Internet Source	<1 %
50	www.intechopen.com Internet Source	<1 %
51	www.jkcs.or.kr Internet Source	<1 %
52	Meimei Wang, Kuihua Han, Jianhui Qi, Zhaocai Teng, Jigang Zhang, Ming Li. "Study on performance and charging dynamics of N/O codoped layered porous carbons derived from L-tyrosine for supercapacitors", Applied Surface Science, 2021	<1 %

Publication

53	Jintao Zhang. "On the Configuration of Supercapacitors for Maximizing Electrochemical Performance", ChemSusChem, 04/30/2012 Publication	<1 %
54	Peng Wan, Zhong Jie Zhang, Wen Mei Song, Min Wang, Xiang Ying Chen, Peng Peng Chen. "Low-temperature and pressure-promoted synthesis of porous carbon modified with oxygen for supercapacitor application", Ionics, 2020 Publication	<1 %
55	Weiwei Qiu, Jialin Zhao, Xuedan Song, Qing Mao, Suzhen Ren, Ce Hao, Yonghou Xiao. "One-Step Activation Synthesized Hierarchical Porous Carbon Spheres from Resorcinol–Thiourea–Formaldehyde for Electrochemical Capacitors", Industrial & Engineering Chemistry Research, 2019 Publication	<1 %

Exclude quotes	Off	Exclude matches	Off
Exclude bibliography	Off		